J. Am. Soc. Mass Spectrom. (2019) 30:796–805
DOI: 10.1007/s13361-019-02179-6

RESEARCH ARTICLE

# Gas-Phase Deconstruction of $UO_2^{2+}$: Mass Spectrometry Evidence for Generation of $[OU^{VI}CH]^+$ by Collision-Induced Dissociation of $[U^{VI}O_2(C{\equiv}CH)]^+$

Michael J. van Stipdonk,[1] Irena J. Tatosian,[1] Anna C. Iacovino,[1] Amanda R. Bubas,[1,2] Luke J. Metzler,[1] Mary C. Sherman,[1] Arpad Somogyi[3]

[1]Department of Chemistry and Biochemistry, Duquesne University, 600 Forbes Avenue, Pittsburgh, PA 15282, USA
[2]*Present Address:* Department of Chemistry, University of Utah, 315 1400 E, Salt Lake City, UT 84112, USA
[3]Mass Spectrometry and Proteomics Facility, Campus Chemical Instrument Center, The Ohio State University, Columbus, OH 43210, USA

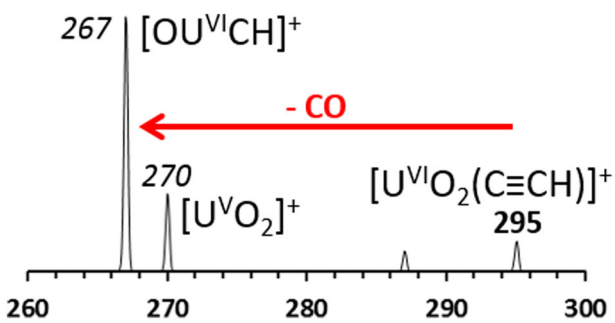


**Abstract.** Because of the high stability and inertness of the U=O bonds, activation and/or functionalization of $UO_2^{2+}$ and $UO_2^+$ remain challenging tasks. We show here that collision-induced dissociation (CID) of the uranyl-propiolate cation, $[U^{VI}O_2(O_2C\text{-}C{\equiv}CH)]^+$, can be used to prepare $[U^{VI}O_2(C{\equiv}CH)]^+$ in the gas phase by decarboxylation. Remarkably, CID of $[U^{VI}O_2(C{\equiv}CH)]^+$ caused elimination of CO to create $[OU^{VI}CH]^+$, thus providing a new example of a well-defined substitution of an "yl" oxo ligand of $U^{VI}O_2^{2+}$ in a unimolecular reaction. Relative energies for candidate structures based on density functional theory calculations suggest that the $[OU^{VI}CH]^+$ ion is a uranium-methylidyne product, with a U≡C triple bond composed of one σ-bond with contributions from the U *df* and C *sp* hybrid orbitals, and two π-bonds with contributions from the U *df* and C *p* orbitals. Upon isolation, without imposed collisional activation, $[OU^{VI}CH]^+$ appears to react spontaneously with $O_2$ to produce $[U^VO_2]^+$.

**Keywords:** Uranyl ion, Collision-induced dissociation, Ion trap mass spectrometry, Oxo ligand substitution, Density functional theory

Received: 28 November 2018/Revised: 4 March 2019/Accepted: 5 March 2019/Published Online: 25 March 2019

## Introduction

While there is growing interest in methods to activate and/or functionalize $UO_2^{2+}$ and $UO_2^+$ [1–3], these transformations remain challenging because of the high (thermodynamic) stability and (kinetic) inertness of the U=O bonds. Despite this, it has been demonstrated that activation and functionalization of U=O bonds can be achieved in the condensed phase using a combination of coordination by Lewis acids and reductive silylation [4–15], or by other means [16–18]. In the gas phase, recent experiments have shown that the U=O bonds of $UO_2^{2+}$ can be activated and substituted, primarily through the use of collision-induced dissociation (CID) [19–23]. For example, we have shown that $NUO^+$ can be created by rearrangement and fragmentation of $[UO_2(N{\equiv}C)]^+$, which was itself generated by dissociation of a $[UO_2(N{\equiv}C\text{-}CH_3)]^{2+}$ precursor [19]. In similar studies, Gibson and coworkers demonstrated that CID of $[UO_2(N_3)Cl_2]^-$ creates the activated ion $[UO(NO)Cl_2]^-$ by elimination of $N_2$ [20], and that $[UO_2(NCO)Cl_2]^-$ will dissociate by elimination of $CO_2$ to leave $[UONCl_2]^-$ [21]. More recent experiments have demonstrated that CID of uranyl complexes with octadentate catecholamide ligands can cause U=O bond cleavage [22], and that $[UO(F)_4]^-$ is the dominant product ion generated by CID of $[UO_2(O_2C\text{-}CF_3)_2]^-$ [23].

**Electronic supplementary material** The online version of this article (https://doi.org/10.1007/s13361-019-02179-6) contains supplementary material, which is available to authorized users.

*Correspondence to:* Michael Stipdonk; *e-mail:* vanstipdonkm@duq.edu

Recently, the gas-phase dissociation reactions of a series of $[AnO_2(O_2C{-}R)_3]^-$, An = U, Np, Pu, precursors were investigated [24]. For precursors containing U, decarboxylation products with general composition $[(R)AnO_2(O_2C{-}R)_2]^-$, species which include discrete U–C organouranyl bonds, were created when R=$CH_3$, $C_6H_5$, $C_6F_5$, $CH_3C{\equiv}C$. In contrast, it was only for R=$C_6F_5$ and $CH_3C{\equiv}C$ that similar species were observed when investigating precursors that contained Np and Pu. The formation of organometallic products was confirmed using infrared multiple-photon photodissociation spectroscopy, and the intrinsic stability of the organoactinyl bonds was investigated by measuring relative gas-phase hydrolysis rates.

We have continued to explore the intrinsic unimolecular reactions of gas-phase organo-uranyl complexes [25]. We report here a study that involved CID of the uranyl-propiolate cation, $[U^{VI}O_2(O_2C\text{-}C{\equiv}C\text{-}H)]^+$. CID of $[U^{VI}O_2(O_2C\text{-}C{\equiv}C\text{-}H)]^+$ was used to prepare the organometallic species $[UO_2(C{\equiv}CH)]^+$ by decarboxylation. Surprisingly, we found that the dominant product ion generated by CID of $[U^{VI}O_2(C{\equiv}CH)]^+$ is $[U^{VI}OCH]^+$, which must be created by the elimination of CO. Experimental data to support the proposed dissociation reaction pathway, including high-accuracy mass to charge ratio (*m/z*) measurements, and preliminary quantum chemical calculations to probe possible structures, chemical bonding, and reaction energetics are presented below.

## Experimental Methods

### *Sample Preparation*

Methanol ($CH_3OH$) and ethanol ($CH_3CH_2OH$) were purchased from Sigma-Aldrich Chemical (St. Louis, MO) and used as received. The sample used to prepare gas-phase $[U^{VI}O_2(O_2C\text{-}C{\equiv}CH)]^+$ was created by combining 2–3 mg of $U^{VI}O_3$ (Strem Chemicals, Newburyport, MA), corresponding to approximately $7 \times 10^{-6}$ to $1 \times 10^{-5}$ mol, with a 2-fold mole excess of propiolic acid (Sigma-Aldrich, St. Louis, MO) and 400 μL of deionized/distilled $H_2O$ in a glass scintillation vial. The solutions were allowed to incubate on a hot plate at 70 °C for 12 h. *Caution: uranium oxide is radioactive (α- and γ-emitter), and proper shielding, waste disposal, and personal protective gear should be used when handling the material.* When cooled, 20 μL of the resulting solution was diluted with 800 μL of 90:10 (by volume) $H_2O/CH_3OH$ or $H_2O/CH_3CH_2OH$ (same proportions) and used without further work up as the spray solution for electrospray ionization (ESI).

ESI and CID experiments were performed on a ThermoScientific (San Jose, CA) LTQ-XL linear ion trap (LIT) mass spectrometer. Solutions for ESI were infused into the instrument using the incorporated syringe pump at a flow rate of 5 μL/min. In the positive ion mode, the auto-tune routine within the LTQ Tune program was used to optimize the atmospheric pressure ionization stack settings for the instrument (lens voltages, quadrupole and octopole voltage offsets, etc.) to achieve maximum transmission of singly charged ions such as $[UO_2(O_2C\text{-}C{\equiv}CH)(H_2O)_2]^+$ and $[UO_2(O_2C\text{-}C{\equiv}CH)(CH_3OH)_2]^+$ to the LIT. Helium was used as the bath/buffer gas to improve trapping efficiency and as the collision gas for CID experiments.

For multiple-stage ($MS^n$) CID experiments to probe fragmentation and ion-molecule reaction (IMR) pathways [26], precursor ions were isolated using a width of 1.0 to 1.5 mass to charge (*m/z*) units. The exact value was determined empirically to provide maximum ion intensity while ensuring isolation of a single isotopic peak. To probe CID behavior, the (mass) normalized collision energy (NCE, as defined by ThermoScientific) was set between 5 and 18%, which corresponds to 0.075–0.27 V applied for CID with the current instrument calibration. The activation Q, which defines the frequency of the applied radio frequency potential, was set at 0.30 and a 30-ms activation time was used.

To probe gas-phase reactions of selected precursor ions with background neutrals (primarily $H_2O$ and $O_2$ [27–29]), ions were isolated using widths of 1–2 *m/z* units. Here too, the specific width was chosen empirically to ensure maximum ion isolation efficiency. The ions were then stored in the LIT for periods ranging from 1 ms to 10 s. While we have shown that the levels of adventitious $H_2O$ in the 2-D LIT, under normal operating conditions, is lower than in 3-D ion traps [19, 30, 31], there is still a sufficient partial pressure to permit an investigation of IMRs, especially when using long isolation times. When examining IMRs, our intent was not to measure or report rates or rate constants, but to identify the *pathways* by which ions react with neutrals such as $H_2O$ or $O_2$ in the LIT. The levels of these neutral species in the LIT are too low to allow a rigorous examination of $H_2O$ addition rates to specific uranyl complexes for comparison to earlier studies, and our instrument is not configured to allow controlled addition of neutral reagents for IMR. For both CID and IMR experiments, the mass spectra displayed were created by accumulating and averaging at least 30 isolation, dissociation, and ejection/detection steps.

High-resolution/high-accuracy measurements were performed on a ThermoScientific (San Jose, CA) LTQ-Orbitrap Elite mass spectrometer using experimental conditions and settings similar to those outlined above for the LTQ-XL instrument. With the Orbitrap instrument, the experiments were performed with the 120,000 resolution setting, NCE values of 8–16%, activation Q setting of 0.25, and a 10-ms activation time. Mass spectra were collected for 1 min at each $MS^n$ stage.

### *Density Functional Theory Calculations*

Geometry optimizations for potential product ion structures were performed using the B3LYP [32–34], PBE0 [35, 36], and M06-2X [37] functionals, the MWB60 pseudopotential and associated basis set on U, and the 6-311+G(d,p) basis set

on all other atoms. In all cases, an ultrafine integration grid was used. Vibrational frequency calculations were used to determine whether optimized structures were true minima (i.e., no imaginary frequencies) and for zero-point and thermal correction of electronic energies. The Gaussian 09 software package [38] was used for all calculations. NBO 5.9, as integrated in the Gaussian 09 software, was used for natural bond orbital (NBO) and natural localized molecular orbital (NLMO) calculations to examine bonding orbital interactions [39].

## Results and Discussion

### *Collision-Induced Dissociation of Water- and Alcohol-Coordinated $[U^{VI}O_2(O_2C\text{-}C{\equiv}CH)]^+$*

The initial goal of this study was to determine whether $[U^{VI}O_2(C{\equiv}CH)]^+$ could be synthesized in the gas phase by decarboxylation (an approach used successfully in prior investigations of metal-carboxylate complexes [24, 40–44]), and to probe the dissociation and IMR reactivity of the species. The ESI mass spectrum generated using a solution created by digestion of $UO_3$ with propiolic acid is shown in Figure 1. The solvent mixture used in this case was 90:10 $H_2O/CH_3OH$, and the most abundant positively charged ions generated were $[U^{VI}O_2(O_2C\text{-}C{\equiv}CH)(H_2O)_2]^+$, $[U^{VI}O_2(O_2C\text{-}C{\equiv}CH)(H_2O)(CH_3OH)]^+$, and $[U^{VI}O_2(O_2C\text{-}C{\equiv}CH)(CH_3OH)_2]^+$ at *m/z* 375, 389, and 403, respectively. The remaining cations observed in the *m/z* 250–370 region of the ESI spectrum are $H_2O$ and MeOH adducts to $[U^{VI}O_2(OH)]^+$ and $[U^{VI}O_2(OCH_3)]^+$ and their CID pathways were investigated in an earlier study [45].

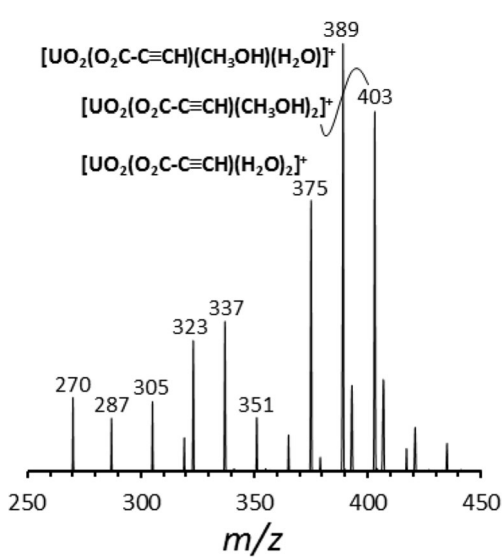


**Figure 1.** Electrospray ionization mass spectrum generated using spray solution of $[UO_2(O_2C\text{-}C{\equiv}CH)_2]$ in 90:10 (*v/v*) $H_2O/CH_3OH$. Compositions of the principal species germane to this study are labeled. Species in the *m/z* region of 250–370 correspond to $H_2O$ and $CH_3OH$-coordinated $[UO_2]^+$, $[UO_2(OH)]^+$, and $[UO_2(OCH_3)]^+$

The CID of $[U^{VI}O_2(O_2C\text{-}C{\equiv}CH)(H_2O)(CH_3OH)]^+$ (data not shown) and $[U^{VI}O_2(O_2C\text{-}C{\equiv}CH)(CH_3OH)_2]^+$ (Figure S1b of the supporting information) led to formation of $[U^{VI}O_2(O_2C\text{-}C{\equiv}CH)(CH_3OH)]^+$ by elimination of an $H_2O$ or MeOH ligand, respectively. In both cases, subsequent CID of $[U^{VI}O_2(O_2C\text{-}C{\equiv}CH)(CH_3OH)]^+$ ($MS^3$ stage, Figure S1c of the supporting information) produced $[U^{VI}O_2(OCH_3)]^+$ by intra-complex proton transfer and elimination of propiolic acid (reaction 1), as well as $[U^{VI}O_2(O_2C\text{-}C{\equiv}CH)]^+$ by elimination of $CH_3OH$ (reaction 2).

$$[U^{VI}O_2(O_2C{-}C{\equiv}CH)(CH_3OH)]^+ \rightarrow [U^{VI}O_2(OCH_3)]^+ + HO_2C{-}C{\equiv}CH \quad (1)$$

$$[U^{VI}O_2(O_2C{-}C{\equiv}CH)(CH_3OH)]^+ \rightarrow [U^{VI}O_2(O_2C{-}C{\equiv}CH)]^+ + CH_3OH \quad (2)$$

The tendency to eliminate propiolic acid over the remaining alcohol ligand was greater for CID of $[U^{VI}O_2(O_2C\text{-}C{\equiv}CH)(CH_3CH_2OH)]^+$ (Figure S2c of the supporting information).

CID of $[U^{VI}O_2(O_2C\text{-}C{\equiv}CH)(H_2O)_2]^+$ at *m/z* 375 generated the highest yield of $[U^{VI}O_2(O_2C\text{-}C{\equiv}CH)]^+$, and is therefore used to summarize the results of the $MS^n$ CID experiments (Figure 2). As shown in Figure 2a, b, CID of $[U^{VI}O_2(O_2C\text{-}C{\equiv}CH)(H_2O)_2]^+$ caused elimination of single $H_2O$ ligands in sequential steps (MS/MS and $MS^3$ stages, respectively) to generate $[U^{VI}O_2(O_2C\text{-}C{\equiv}CH)]^+$ at *m/z* 339. Subsequent CID of $[U^{VI}O_2(O_2C\text{-}C{\equiv}CH)]^+$ ($MS^4$ stage, Figure 2c) generated peaks initially assigned as $[U^{VI}O_2(C{\equiv}CH)]^+$ at *m/z* 295, and $[U^{VI}O_2(OH)]^+$ at *m/z* 287.

The $[U^{VI}O_2(C{\equiv}CH)]^+$ ion at *m/z* 295 was isolated, independently, for IMR in the LIT for periods ranging from 1 ms to 1 s ($MS^5$ stage, Figure S3a–d of the supporting information). It is important to note that during the isolation step, all ionized species except the one chosen for storage are resonantly ejected from the ion trap. The appearance of peaks other than the isolated ion identifies IMR products. The isolation and storage of $[U^{VI}O_2(C{\equiv}CH)]^+$ in the LIT led to production of $[U^{VI}O_2(OH)]^+$ at *m/z* 287. The neutral eliminated in the reaction is assumed to be acetylene (reaction 3), which indicates a gas-phase IMR with background $H_2O$. Therefore, it is likely that the $[U^{VI}O_2(OH)]^+$ product that appears in the CID spectrum of $[U^{VI}O_2(O_2C\text{-}C{\equiv}CH)]^+$ (Figure 2c) is generated by hydrolysis of $[U^{VI}O_2(C{\equiv}CH)]^+$ after its creation by decarboxylation. This general pattern in reactivity is consistent with our earlier study of the formation of uranyl-organometallic complexes [24].

$$[U^{VI}O_2(C{\equiv}CH)]^+ + H_2O \rightarrow [U^{VI}O_2(OH)]^+ + HC{\equiv}CH \quad (3)$$

In our previous study, CID of the positively charged organometallic uranyl species such as $[U^{VI}O_2(CH_3)]^+$ and $[U^{VI}O_2(CH_2CH_3)]^+$ generated $[U^{V}O_2]^+$ by elimination of (neutral) methyl and ethyl radicals, respectively [25]. In the

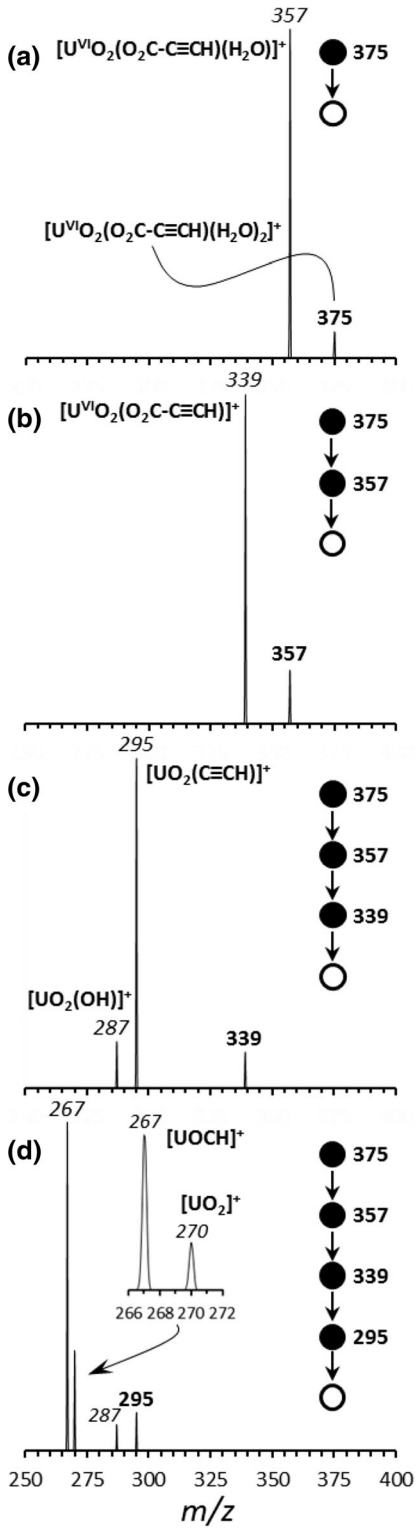


**Figure 2.** Multiple-stage CID spectra initiated with $[UO_2(O_2C\text{-}C{\equiv}CH)(H_2O)_2]^+$: (**a**) CID (MS/MS stage) of $[UO_2(O_2C\text{-}C{\equiv}CH)(H_2O)_2]^+$, (**b**) CID ($MS^3$ stage) of $[UO_2(O_2C\text{-}C{\equiv}CH)(H_2O)]^+$, (**c**) CID ($MS^4$ stage) of $[UO_2(O_2C\text{-}C{\equiv}CH)]^+$, and (**d**) CID ($MS^5$ stage) of $[UO_2(C{\equiv}CH)]^+$. For the spectra, the circles and arrows illustrate the $MS^n$ sequence/pathway. In each spectrum, the bold peak label indicates the precursor selected for CID whereas labels in italics represent the products from dissociation or ion-molecule reactions as indicated in the text

present set of experiments, however, subsequent CID of $[U^{VI}O_2(C{\equiv}CH)]^+$ at *m/z* 295 ($MS^5$ stage, Figure 2d) generated a peak at *m/z* 267, along with $[U^{V}O_2]^+$ and $[U^{IV}O_2(OH)]^+$ at *m/z* 270 and 287, respectively. The ion at *m/z* 267 was initially assigned as $[UOCH]^+$, which would be formed by the elimination of CO upon collisional activation of $[U^{VI}O_2(C{\equiv}CH)]^+$.

The LIT does not have sufficient mass measurement accuracy to unambiguously establish molecular formulae for the ions at *m/z* 267 and 239. However, the LTQ-Orbitrap instrument is capable of resolving powers greater than 100,000 (m/Δm), and accuracies in the 1–5-ppm range. Accurate masses measured with the LTQ-Orbitrap are compared to theoretical monoisotopic masses for a range of possible precursor and product ion compositions in Table S1 of the supporting information. For the species at nominal *m/z* 339, assumed to be $[U^{VI}O_2(O_2C\text{-}C{\equiv}CH)]^+$, the accurate *m/z* value differs from the theoretical mass for the corresponding molecular formula of $[C_3HO_4U]$ by 0.200 mDa (0.590 ppm error) and supports the composition assignment. The same is true for the ion at nominal *m/z* 295, assumed to be $[UO_2(C{\equiv}CH)]^+$ for which the measured mass differs from the theoretical mass by 0.300 mDa (1.017 ppm error) for the molecular formula $[C_2HO_2U]$. In addition, the difference in measured mass between $[C_3HO_4U]$ and $[C_2HO_2U]$ is 43.9899 u compared to the theoretical mass for $CO_2$ of 43.9898 (0.100 mDa difference, 2.273 ppm error). This provides additional support for a dissociation reaction that involves elimination of $CO_2$ from $[U^{VI}O_2(O_2C\text{-}C{\equiv}CH)]^+$ to create $[U^{VI}O_2(C{\equiv}CH)]^+$. The accurate mass measurements also support the composition assignments for the *m/z* 287, 286, and 270 ions ($[U^{VI}O_2(OH)]^+$, $[U^{VI}O_2(O)]^+$, and $[U^{V}O_2]^+$, respectively).

The accurate mass measurement for the ion at nominal *m/z* 267 differs from the theoretical mass for a composition of $[UOCH]^+$ by only 0.400 mDa (1.498 ppm error). Furthermore, the difference in measured masses of $[U^{VI}O_2(C{\equiv}CH)]^+$ and $[UOCH]^+$ is 27.9950 u compared to a theoretical mass for CO of 27.9949 (0.100 mDa, 3.572 ppm error). Clearly, the accurate mass measurements support the hypothesis that sequential CID steps cause the decarboxylation of $[U^{VI}O_2(O_2C\text{-}C{\equiv}CH)]^+$ to create $[U^{VI}O_2(C{\equiv}CH)]^+$ and, more importantly, subsequent elimination of CO to leave $[UOCH]^+$.

Given the established compositions of the precursor and product ions, we can speculate on the general $MS^n$ CID pathways initiated with the $[U^{VI}O_2(O_2C\text{-}C{\equiv}CH)(H_2O)_2]^+$ precursor, and by extension, the alcohol-coordinated analogues. Scheme 1 shows a proposed sequence of steps. At the MS/MS stage, CID causes the elimination of a single $H_2O$ or ROH ($R{=}CH_3$ or $CH_2CH_3$) ligand. Elimination of an alcohol ligand competes with intra-complex proton transfer and elimination of (neutral) propiolic acid at the $MS^3$ stage. The loss of propiolic acid is most favored for complexes that include $CH_3CH_2OH$, less so for analogues that contain $CH_3OH$ and is not observed

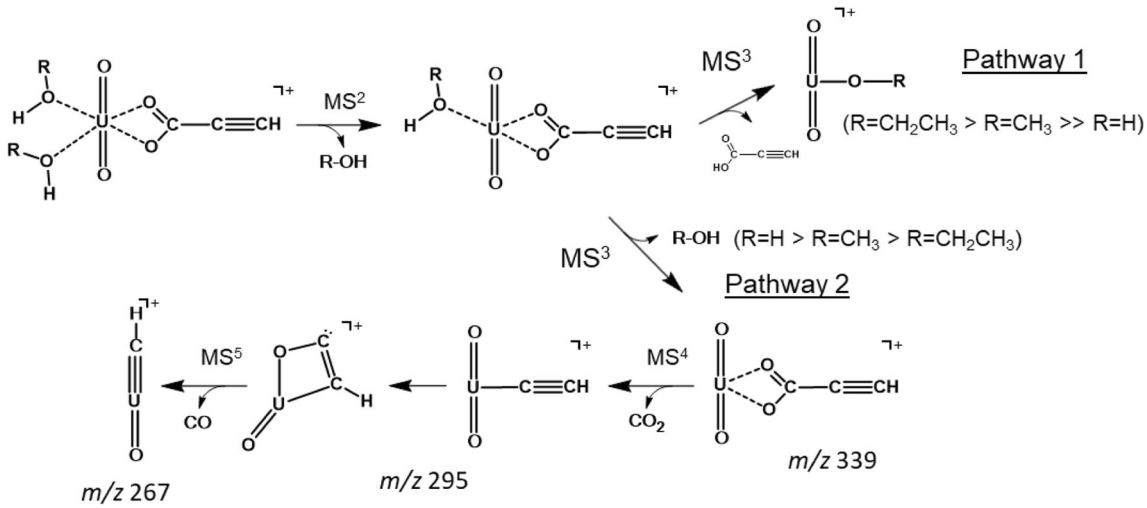


**Scheme 1.** Reaction pathway to production of $[OUCH]^+$ by multiple-stage CID of $[UO_2(O_2C\text{-}C{\equiv}CH)(R\text{-}OH)_2]^+$ (R=H, $CH_3$, or $CH_2CH_3$)

for $[U^{VI}O_2(O_2C\text{-}C{\equiv}CH)(H_2O)_2]^+$. We note that in these experiments, the tendency to eliminate neutral propiolic acid and retain hydroxide or alkoxide follows the relative trend in gas-phase acidity, $CH_3CH_2OH > CH_3OH > H_2O$ [46, 47]. Upon loss of the second $H_2O$ or ROH ligand ($MS^3$ stage), subsequent CID of $[U^{VI}O_2(O_2C\text{-}C{\equiv}CH)]^+$ causes decarboxylation to generate $[U^{VI}O_2(C{\equiv}CH)]^+$. We propose that elimination of CO from $[U^{VI}O_2(C{\equiv}CH)]^+$ may occur by rearrangement and nucleophilic attack by an "yl" oxo ligand.

## *Computed Structures for $[OUCH]^+$*

The composition assignment of $[OUCH]^+$ leads to the intriguing suggestion that a uranium-methylidyne (i.e., -U≡CH) species is generated by CID of $[U^{VI}O_2(C{\equiv}CH)]^+$. Formation of similar species, such as (neutral) $[F_3U^{VI}CH]$, has been reported by Andrews, Li, and coworkers in experiments that involved reactions of laser-ablated U atoms with trihalomethanes or carbon tetrafluoride [48]. Following deposition of gas-phase species into an Ar matrix at 8 K, annealing and irradiation with UV light, a range of products were identified using infrared spectroscopy and density functional theory (DFT) calculations. Beyond data from vibrational spectra, support for generation of a methylidyne in the matrix-isolation studies was provided by quantum mechanical calculations and NLMO, which suggest the formation of a triple bond between uranium and carbon: one σ-bond utilizing the U *df* and C *sp* hybrid orbitals, and two π-bonds utilizing the U *df* and C *p* orbitals [48].

Despite the information provided by the $MS^n$ CID patterns and accurate mass measurements in the present study, the

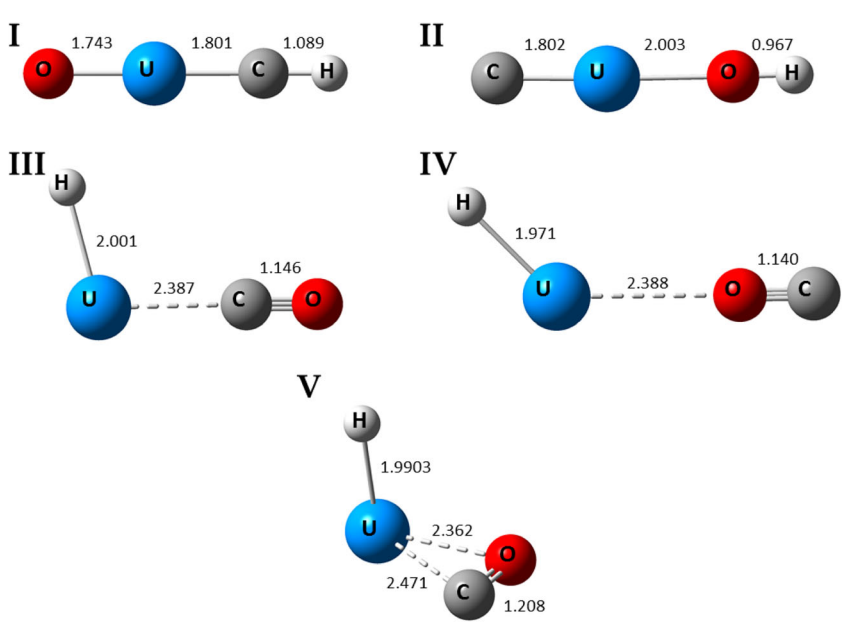


**Figure 3.** Possible structures for product ion at *m/z* 267, with composition [OUCH]. Structure were generated from calculations at the B3LYP/MWB60/6-11+G(d,p) level of theory. Bond lengths are shown in angstroms

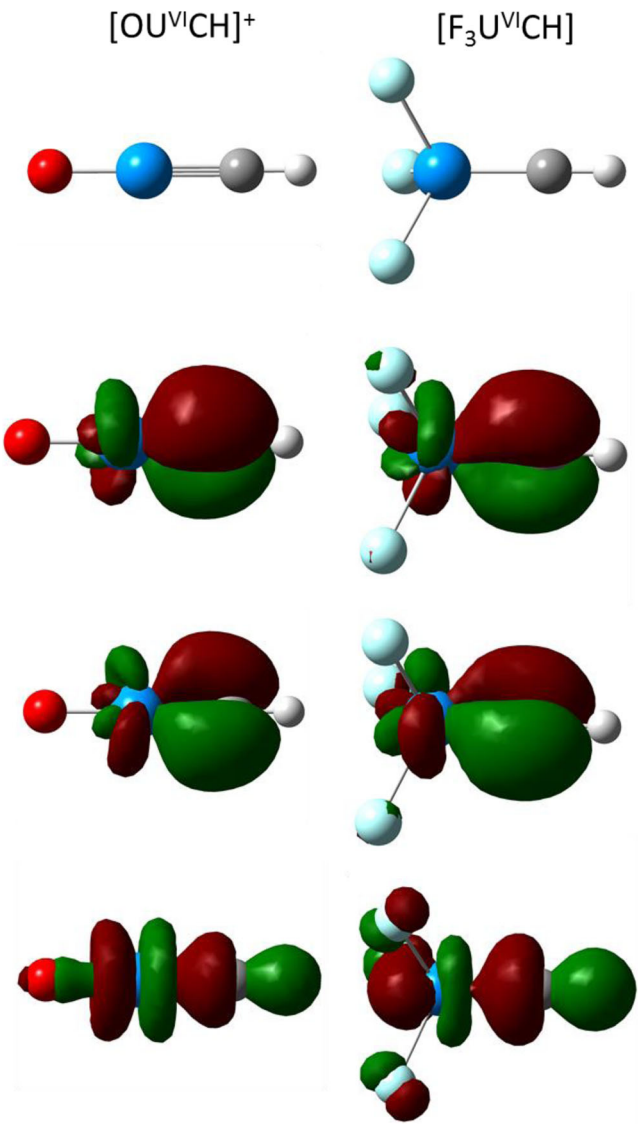


**Figure 4.** Bonding orbitals for $[OU^{VI}CH]^+$ and $[F_3U^{VI}CH]$, generated at the B3LYP/MWB60/6-11+G(d,p) level of theory

structure of the ion at nominal *m/z* 267 is not known. Therefore, DFT calculations were used to predict possible connectivity and structures for the product ion, and 5 minima were identified (structures **I**–**V** in Figure 3). Structure **I** is the methylidyne structure with connectivity [O-U-C-H]. The connectivity of structure **II** is instead [C-U-O-H]. Structures **III** through **V** are best described as $[U\text{-}H]^+$ coordinated to CO: structures **III** and **IV** are end-on complexes with coordination of U by either O or C, while structure **V** is an $\eta^2$ complex with CO bound side-on.

The electronic energies, zero-point corrections, and relative energies in kilojoules/mole for the respective structures, modeled in both the singlet and triplet spin states, are provided in Table S2 of the supporting information. The computed energy for the [O-U-C-H] composition/structure is significantly lower in energy than the other minima identified, regardless of the functional used. The calculations also suggest that the singlet state is lowest in energy for the [O-U-C-H] composition (structure **I**) while the triplet state is favored for the [C-U-O-H] and [H-U-CO] species (structures **II** through **V**). We tentatively conclude, therefore, that the ion at *m/z* 267 corresponds to $[O\text{-}U\text{-}C\text{-}H]^+$, with the caveat that any potential barriers to the rearrangements necessary to generate the respective species have been neglected in our argument. However, based on the calculated relative energies, we feel that it is reasonable to assume that the $[OU^{VI}CH]^+$ ion adopts the linear geometry of structure **I**.

We next examined the (calculated) molecular orbitals and atomic charges for $[OU^{VI}CH]^+$. Of particular interest was the evidence for a U-C triple bond, and correlation between the bonding in $[OUCH]^+$ to similar structures identified by Andrews and coworkers [48]. As noted above, the (neutral) species $[F_3U^{VI}CH]$ is proposed to include a U-C triple bond, and it was noted by Andrews and Li that strong inductive effects of the fluoride ligands support the positive charge on U, which stabilizes the U(VI) oxidation state and, in turn, the bonding to the methylidyne ligand. The molecular orbitals for $[OU^{VI}CH]^+$ and $[F_3U^{VI}CH]$, calculated here using the same functional and basis set to facilitate direct comparison, are shown in Figure 4.

The bonding patterns for the two species are nearly identical at the level of theory used, including formation of a triple bond by σ-bonding involving the U *df*σ and C *sp*σ hybrid orbitals, and two π-bonds between the U*df*π and C*p*π orbitals. A comparison of the natural charges on U and C, the Wiberg natural bond order ($BO_w$), NBO occupancies, and NLMO compositions are shown in Table 1. The electron contributions from carbon and uranium to form the U-C σ-bonding NLMO, 53 and 45%, respectively, indicate a higher degree of covalent character in $[OU^{VI}CH]^+$ than in $[F_3U^{VI}CH]$ (71 and 29%, respectively). The slightly higher bond order in $[OU^{VI}CH]^+$ is likely due to the higher occupancy of the two π-bonding orbitals, provided by favorable overlap with the *p*-bonding orbitals of the oxo ligand. In addition, the stabilizing inductive effect attributed to the fluoride ligands in $[F_3U^{VI}CH]$ is provided in the case of

**Table 1.** Natural Charges on Uranium ($q_u$) and Carbon ($q_c$), Wiberg Natural Bond Order ($BO_w$) for the U-C Bond, Occupancies of the U-C NBOs, and the Contributions of Both Uranium and Carbon to the Bonding NLMOs. Hybridization Values for Uranium Are Normalized with Respect to the d-Orbital Contributions

| | $q_U$ | $q_C$ | $BO_W$ | | NBO occupancy | NLMO contributions & hybrids | |
|---|---|---|---|---|---|---|---|
| $[OU{\equiv}CH]^+$ | 2.04 | −0.61 | 2.83 | σ | 1.87 | 53%[a] C ($s^1$ $p^{0.80}$) | 45%[a] U ($s^{0.06}$ $p^{0.09}$ $d^{1.00}$ $f^{2.92}$) |
| | | | | π | 1.97 | 55% C ($p^{1.00}$) | 45% U ($p^{0.03}$ $d^{1.00}$ $f^{1.77}$) |
| $[F_3U{\equiv}CH]$ | 1.89 | −0.41 | 2.78 | σ | 1.95 | 71% C ($s^1$ $p^{0.62}$) | 29% U ($s^{0.12}$ $d^{1.00}$ $f^{0.57}$) |
| | | | | π | 1.88 | 46% C ($p^{1.00}$) | 54% U ($p^{0.01}$ $d^{1.00}$ $f^{4.41}$) |

[a]A significant (2%) delocalization contribution from the -yl oxygen brings the total to 100%

**Table 2.** Computed Gibbs Free Energies for Reactions 4–7. Calculations Were Performed Using the B3LYP, M06-2X, and PBE0 Functionals, MWB60 Pseudopotential and Basis Set on U, and 6-311+G(d,p) Basis Set on C, H, and O

| | ΔG (kJ/mol) | | |
|---|---|---|---|
| | B3LYP | M06-2X | PBE0 |
| $[U^{VI}O_2(C{\equiv}CH)]^+ \rightarrow [U^{V}O_2]^+ + C{\equiv}CH$ | 253.3 | 255.1 | 231.8 |
| $[U^{VI}O_2(C{\equiv}CH)]^+ \rightarrow [OU^{VI}CH]^+ + CO$ | 215.1 | 165.8 | 213.2 |
| | ΔG (kJ/mol) | | |
| | B3LYP | M06-2X | PBE0 |
| $[OU^{VI}CH]^+ + O_2 \rightarrow [U^{V}O_2]^+ + OCH$ | − 604.2 | − 555.7 | − 596.5 |
| $[OU^{VI}CH]^+ + H_2O \rightarrow [U^{V}O_2]^+ + CH_3$ | − 279.1 | − 217.4 | − 260.1 |

$[OU^{VI}CH]^+$ by the oxo ligand, as indicated by the small, but significant, contribution to the U-C σ-bonding NLMO.

As noted above, our previous study showed that CID of $[U^{VI}O_2(CH_3)]^+$ and $[U^{VI}O_2(CH_2CH_3)]^+$ generated $[U^{V}O_2]^+$ by elimination of (neutral) methyl and ethyl radicals, respectively [25]. Therefore, another consideration in the present study was competition between rearrangement of $[U^{VI}O_2(C{\equiv}CH)]^+$ and loss of CO to create $[OU^{VI}CH]^+$ (reaction 4) and direct ejection of C≡CH radial to leave $[U^{V}O_2]^+$ (reaction 5), especially because a peak corresponding to $[U^{V}O_2]^+$ appears in Figure 2d at ca. 20% relative intensity.

$$\left[U^{VI}O_2(C{\equiv}CH)\right]^+ \rightarrow \left[OU^{VI}CH\right]^+ + CO \quad (4)$$

$$\left[U^{VI}O_2(C{\equiv}CH)\right]^+ \rightarrow \left[U^{V}O_2\right]^+ + C{\equiv}CH \quad (5)$$

The computed Gibbs free energies for reactions 4 and 5 are provided in Table 2. As expected, both reactions are predicted to be endergonic. However, the computed energies suggest that reaction 4 requires less energy and should be favored over reaction 5. Therefore, the DFT results are consistent with the experimental observation that rearrangement and loss of CO is favored over elimination of C≡CH radical.

## *Apparent ion-molecule reactions of $[OU^{VI}CH]^+$*

The isolation, without imposed collisional activation, of $[OU^{VI}CH]^+$ was investigated to determine the susceptibility of the species to reactions with neutrals in the ion trap. The LIT is not currently configured to allow the controlled introduction of neutral reagents for accurate measurements of ion reaction rates. Previous studies done by our group and others have demonstrated that gas-phase organometallic species, including those that contain $U^{VI}$ and $U^{V}$, will undergo hydrolysis reactions [30, 31, 42–44], and there is a pronounced tendency for $U^{V}$ species to add molecular oxygen [28, 49–51]. Both $H_2O$ and $O_2$ are present in sufficient quantities as background gases to probe general trends in reactivity.

Product ion spectra generated by isolation and storage of $[OU^{VI}CH]^+$ for 10 ms, 100 ms, and 1 s are shown in Figure 5a–c. At 10-ms reaction time, the only product ion observed above baseline was $[U^{V}O_2]^+$ at *m/z* 270. At 100-ms reaction time, the intensity of $[U^{V}O_2]^+$ increased, and a minor peak at *m/z* 255 was also observed. The ion at *m/z* 255 is consistent with formation of $[U^{II}(OH)]^+$ or $[U^{IV}(O)(H)]^+$ and elimination of $[OCH_2]$. The $[U^{V}O_2]^+$ product was the base peak at 1000 ms isolation time, and a minor peak (< 5% relative intensity) corresponding to formation of $[U^{VI}O_2(OH)]^+$ was also observed.

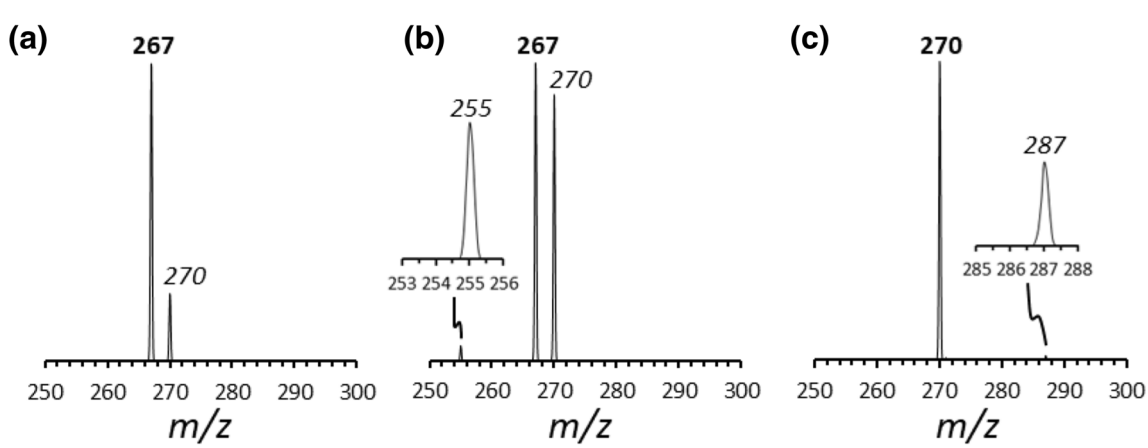


**Figure 5.** Product in spectra generated by isolating $[OU^{VI}CH]^+$, without imposed collisional activation for (**a**) 10 ms, (**b**) 100 ms, and (**c**) 1000 ms. During isolation period, the $[OU^{VI}CH]^+$ ion reacts with adventitious $H_2O$ and/or $O_2$ in the linear ion trap. In each spectrum, the bold peak label indicates the precursor selected for isolation whereas labels in italics represent the products from ion-molecule reactions

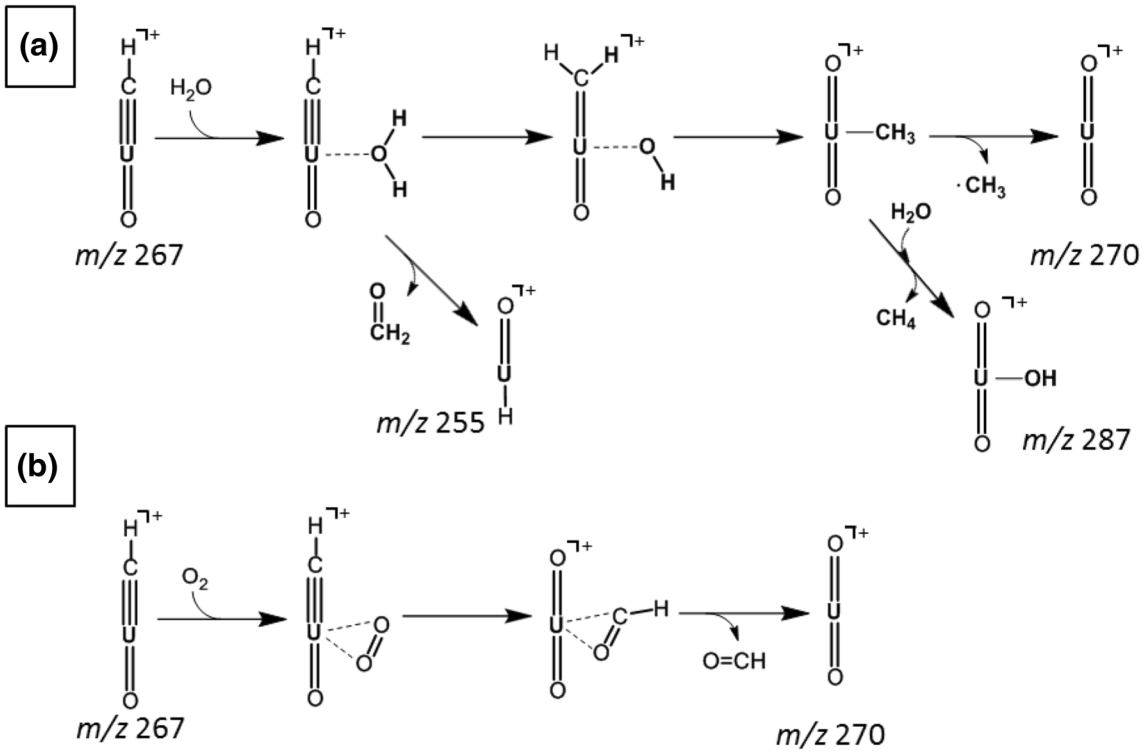


**Scheme 2.** Proposed pathways for ion-molecule reaction between $[OUCH]^+$ and (**a**) background $H_2O$ and (**b**) background $O_2$

Reasonable pathways to explain the apparent reaction of $[OU^{VI}CH]^+$ with $H_2O$ (reaction 6) or $O_2$ (reaction 7) to generate $[U^VO_2]^+$ are provided in Scheme 2.

$$[OU^{VI}CH]^+ + H_2O \rightarrow [U^VO_2]^+ + CH_3 \quad (6)$$

$$[OU^{VI}CH]^+ + O_2 \rightarrow [U^VO_2]^+ + OCH \quad (7)$$

In pathway A (reaction 6), addition of $H_2O$ to $[OU^{VI}CH]^+$, followed by consecutive H transfer steps might yield the organometallic species $[UO_2(CH_3)]^+$, which would then either undergo elimination of methyl radical to leave $UO_2^+$ or hydrolysis to create $[UO_2(OH)]^+$. In pathway B (reaction 7), addition of $O_2$ to $[OU^{VI}CH]^+$, subsequent generation of a formyl anion, and then elimination of OCH radical would also furnish $[U^VO_2]^+$. The computed free energies for reactions 6 and 7 are provided in Table 2. While the DFT calculations suggest that both pathways should be spontaneous, the reaction with $O_2$ is significantly more exergonic. Furthermore, the calculations strongly suggest that $O_2$ addition leads spontaneously to oxidation of the methynyl group to create the formyl anion (structure **VI** in Figure S4), whereas $H_2O$ addition merely creates a hydrate (structure **VII** in Figure S4).

The likelihood that reaction pathway A contributes to the formation of $[U^VO_2]^+$ can be tested, in part, by probing the IMR of $[U^{VI}O_2(CH_3)]^+$, which can be generated independently using CID of $[U^{VI}O_2(OCH_2CH_3)]^+$ [25]. Isolation of $[U^{VI}O_2(CH_3)]^+$ for periods ranging from 10 ms to 10 s ($MS^4$ stage, Figure S5 of the supporting information) leads to formation of $[U^VO_2(H_2O)]^+$ and hydrates of the product. The $[U^VO_2]^+$ ion at *m/z* 270 is observed at only 10% relative intensity, and a peak corresponding to $[U^{VI}O_2(OH)]^+$ at *m/z* 287 is not detected above baseline. Preliminary calculations of reaction energetics (Table S3) suggest that while hydrolysis (reaction 8) should be favored thermodynamically, the barrier for proton transfer to create $CH_4$ is higher than the energy required to eliminate the methyl radical directly (reaction 9).

$$[U^{VI}O_2(CH_3)]^+ + H_2O \rightarrow [U^{VI}O_2(OH)]^+ + CH_4 \quad (8)$$

$$[U^{VI}O_2(CH_3)]^+ + H_2O \rightarrow [U^VO_2(H_2O)]^+ + \bullet CH_3 \quad (9)$$

The data generated by independent isolation and reaction of $[U^{VI}O_2(CH_3)]^+$ is inconsistent with participation of the species as an intermediate in the IMR of $[OU^{VI}CH]^+$ with $H_2O$. If pathway A was to contribute significantly to the reactivity of $[OU^{VI}CH]^+$, we would expect a peak corresponding to $[U^VO_2(H_2O)]^+$ at *m/z* 288 to be present in the product ion spectrum. Because $[U^VO_2]^+$ is the dominant product ion observed, we conclude instead that the formation of $[U^VO_2]^+$ from $[OUCH]^+$ is due to reaction with $O_2$ in the ion trap. While the mechanism remains speculative without isotopic labeling to confirm reactions with $H_2O$ over $O_2$, and comprehensive quantum chemical modeling of the reaction pathways is beyond the scope of this report, our preliminary experiments demonstrate

that the alkylidyne species, if generated, is very reactive in the gas phase and open the door for further studies.

## Conclusions

In summary, we have shown that CID of $[U^{VI}O_2(O_2CC{\equiv}CH]^+$ can be used to prepare the organometallic species $[U^{VI}O_2(C{\equiv}CH)]^+$ by decarboxylation. High-accuracy *m/z* measurements demonstrate conclusively that subsequent CID of $[U^{VI}O_2(C{\equiv}CH)]^+$ caused elimination of (neutral) CO to furnish $[OU^{VI}CH]^+$, thus providing another example of the substitution of an oxo ligand of uranyl ion in a unimolecular gas-phase reaction. Relative energies for various candidate structures based on DFT calculations suggest that the $[OU^{VI}CH]^+$ ion is a uranium-methylidyne product, demonstrating one rare instance of a U≡C triple bond. To the best of our knowledge, there is only one other report of the synthesis of such a species [42].

One limitation of the present study is the lack of clear structural information to support the proposed formation of an alkylidyne species. The DFT calculations provide circumstantial information about the most probable structure, and a reasonable reaction pathway (Scheme 1) involves intramolecular nucleophilic attack by the "yl" oxo ligand of $UO_2^{2+}$ on the C-atom of the alkynyl ligand to leave $[OU^{VI}CH]^+$ as a product.

DFT calculations of $[UO^{VI}CH]^+$ and $[F_3U^{VI}CH]$ [42] were performed here at the same level of theory to allow direct comparison. The bonding patterns for the two species are nearly identical at the level of theory used. The U≡C triple bond formed is composed of one σ-bond with contributions from the U *df* and C *sp* hybrid orbitals, and two π-bonds with contributions from the U *df* and C *p* orbitals. NBO occupancies and NLMO compositions were used in a preliminary probe of chemical bonding. NLMO calculations show electron contributions from carbon and uranium to be 53 and 45%, respectively, indicating a higher degree of covalent character in $[OU^{VI}CH]^+$ than in $[F_3U^{VI}CH]$ (71 and 29%, respectively). We speculate that the slightly higher bond order in $[OU^{VI}CH]^+$ is likely due to the higher occupancy of the two π-bonding orbitals, provided by favorable overlap with the *p* orbitals of the oxo ligand. In addition, the oxo ligand of $[OU^{VI}CH]^+$ appears to provide a stabilizing inductive effect to the complex.

Computed Gibbs free energies also suggest that reaction of $[OU^{VI}CH]^+$ with either $H_2O$ or $O_2$ to create $[U^VO_2]^+$ should be spontaneous. However, the reaction is significantly more exergonic for $O_2$ addition, and the calculations strongly suggest that spontaneous oxidation of the methynyl group to create a formyl anion occurs. Based on this, and data from independent measurements that rules out a presumed intermediate on the pathway for reaction with $H_2O$, we conclude that the formation of $[U^VO_2]^+$ from $[OU^{VI}CH]^+$ is due to reaction with $O_2$ in the ion trap. However, because of the appearance of a minor peak corresponding to $[UOH]^+$ at *m/z* 255, spontaneous reactions of $[OU^{VI}CH]^+$ with $H_2O$ cannot be ruled out altogether. A more comprehensive computational examination of the reaction pathways, including the formation of $[UOH]^+$, is beyond the scope of this study and will be reported at a later date.

## Acknowledgements

M.V.S. acknowledges support for this work in the form of start-up funds from the Bayer School of Natural and Environmental Sciences and Duquesne University. Laboratory space renovation was made possible through support by the National Science Foundation through grant CHE-0963450. Support for this work was also provided by the Robert Dean Loughney Faculty Development Endowment. A.I. and A.B. acknowledge support for summer undergraduate and senior thesis research from Duquesne University and the National Science Foundation (CHE-1221615 and CHE-1263279).

## References

1. Fortier, S., Hayton, T.W.: Oxo ligand functionalization in the uranyl ion ($UO_2^{2+}$). Coord. Chem. Rev. **254**, 197–214 (2010)
2. Baker, R.J.: New reactivity of the uranyl(VI) ion. Chem. Eur. J. **18**, 16258–16271 (2012)
3. Jones, M.B., Gaunt, A.J.: Recent developments in synthesis and structural chemistry of non-aqueous actinide complexes. Chem. Rev. **113**, 1137–1198 (2013)
4. Arnold, P.L., Love, J.B., Patel, D.: Pentavalent uranyl complexes. Coord. Chem. Rev. **253**, 1973–1978 (2009)
5. Graves, C.R., Kiplinger, J.L.: Pentavalent uranium chemistry: synthetic pursuit of a rare oxidation state. Chem. Commun. **26**, 3831–3853 (2008)
6. Sarsfield, M.J., Helliwell, M.: Extending the chemistry of the uranyl ion: Lewis acid coordination to a U=O oxygen. J. Am. Chem. Soc. **126**, 1036–1037 (20014)
7. Arnold, P., Patel, D., Blanke, A.J., Wilson, C., Love, J.B.: Selective oxo functionalization of the uranyl ion with 3d metal cations. J. Am. Chem. Soc. **128**, 9610–9611 (2006)
8. Arnold, P.L., Patel, D., Wilson, C., Love, J.B.: Reduction and selective oxo group silylation of the uranyl dication. Nature. **451**, 315–317 (2008)
9. Arnold, P.L., Pecharman, A.-F., Hollis, E., Yahia, A., Maron, L., Parsons, A., Love, J.B.: Uranyl oxo activation and functionalization by metal cation coordination. Nat. Chem. **12**, 1056–1061 (2010)
10. Arnold, P.L., Hollis, E., Nichol, G.S., Love, J.B., Griveau, J.-C., Caciuffo, R., Magnani, N., Maron, L., Castro, L., Yahia, A., Odoh, S.O., Schreckenback, G.: Oxo-functionalization and reduction of the uranyl ion through lanthanide-element bond hemolysis: synthetic, structural, and bonding analysis of a series of singly reduced uranyl-rare earth 5f1-4fn complexes. J. Am. Chem. Soc. **135**, 3841–3854 (2013)
11. Arnold, P.L., Pecharman, A.-F., Lord, R.M., Jones, G.M., Hollis, E., Nichol, G.S., Maron, L., Fang, J., Davin, T., Love, J.B.: Control of oxo-group functionalization and reduction of the uranyl ion. Inorg. Chem. **54**, 3702–2710 (2015)
12. Schnaars, D.D., Wu, G., Hayton, T.W.: Reduction of pentavalent uranyl to U(IV) facilitated by oxo functionalization. J. Am. Chem. Soc. **131**, 17532–17533 (2009)
13. Hayton, T.W., Wu, G.: Exploring the effects of reduction or Lewis acid coordination on the U=O bond of the uranyl moiety. Inorg. Chem. **48**, 3065–3072 (2009)
14. Schnaars, D.D., Wu, G., Hayton, T.W.: Silylation of the uranyl ion using $B(C_6F_5)_3$-activated $Et_3SiH$. Inorg. Chem. **50**, 9642–9649 (2011)
15. Pedrick, E.A., Wu, G., Kaltsoyannis, N., Hayton, T.W.: Reductive silylation of a uranyl dibenzoylmethanate complex: an example of controlled uranyl oxo ligand cleavage. Chem. Sci. **5**, 3204–3213 (2014)
16. Seaman, L.A., Pedrick, E.A., Wu, G., Hayton, T.W.: Promoting oxo functionalization in the uranyl ion by ligation to ketimides. J. Organomet. Chem. **857**, 34–37 (2018)

17. Pedrick, E.A., Wu, G., Hayton, T.W.: Oxo ligand substitution in a cationic uranyl complex: synergistic interaction of an electrophile and a reductant. Inorg. Chem. **54**, 7038–7044 (2015)
18. Kiernicki, J.J., Cladis, D.P., Fanwick, P.E., Zeller, M., Bart, S.C.: Synthesis, characterization, and stoichiometric U-O bond scission in uranyl species supported by pyridine(diamine) ligand radicals. J. Am. Chem. Soc. **137**, 11115–11125 (2015)
19. Van Stipdonk, M.J., Michelini, M., Plaviak, A., Martin, D., Gibson, J.K.: Formation of bare $UO_2^{2+}$ and $NUO^+$ by fragmentation of gas-phase uranyl-acetonitrile complexes. J. Phys. Chem. A. **118**, 7838–7846 (2014)
20. Gong, Y., Vallet, V., Michelini, M., Rios, D., Gibson, J.K.: Activation of gas-phase uranyl: from and oxo to a nitrido complex. J. Phys. Chem. A. **118**, 325–330 (2014)
21. Gong, Y., de Jong, W.A., Gibson, J.K.: Gas phase uranyl activation: formation of a uranium nitrosyl complex from uranyl azide. J. Am. Chem. Soc. **137**, 5911–5915 (2015)
22. Abergel, R.J., de Jong, W.A., Deblonde, G.J.-P., Dau, P.D., Captain, I., Eaton, T.M., Jian, J., van Stipdonk, M.J., Martens, J., Berden, G., Oomens, J., Gibson, J.K.: Cleaving off uranyl oxygens through chelation: a mechanistic study in the gas phase. Inorg. Chem. **56**, 12930–12937 (2017)
23. Van Stipdonk, M.J., Bubas, A., Tatosian, I., Perez, E., Polonsky, N., Metzler, L., Somogyi, A.: Formation of $[U^{V}OF_4]^-$ by collision-induced dissociation of a $[U^{VI}O_2(O_2)(O_2C\text{-}CF_3)_2]^-$ precursor. Int. J. Mass Spectrom. **424**, 58–64 (2018)
24. Dau, P.D., Rios, D., Gong, Y., Michelini, M.C., Marçalo, J., Shuh, D.K., Mogamman, M., Van Stipdonk, M.J., Corcovilos, T.A., Martens, J.K., Oomens, J., Redlich, B., Gibson, J.K.: Synthesis and hydrolysis of uranyl, neptunyl and plutonyl gas-phase complexes exhibiting discrete actinide-carbon bonds. Organometallics. **35**, 1228–1240 (2016)
25. Van Stipdonk, M.J., Hanley, C., Perez, E., Pestok, J., Mihm, P., Corcovilos, T.A.: Collision-induced dissociation of uranyl-methoxide and uranyl-ethoxide cations: formation of $UO_2H^+$ and uranyl-alkyl product ions. Rapid Comm. Mass Spectrom. **30**, 1879–1890 (2016)
26. O'Hair, R.A.J.: The 3-D quadrupole ion trap mass spectrometer as a complete chemical laboratory for fundamental gas-phase studies of metal mediated chemistry. Chem. Comm. 1469–1481 (2006)
27. Chien, W., Hanna, D., Anbalagan, V., Gresham, G., Groenewold, G., Zandler, M., Van Stipdonk, M.J.: Intrinsic hydration of uranyl-hydroxide, -nitrate and -acetate complexes. J. Am. Soc. Mass Spectrom. **15**, 777–783 (2004)
28. Leavitt, C.M., Bryantsev, V.S., de Jong, W.A., Diallo, M.S., Goddard III, W.A.: Addition of $H_2O$ and $O_2$ to acetone and dimethylsulfoxide ligated uranyl(V) dioxocations. J. Phys. Chem. A. **113**, 2350–2358 (2009)
29. Van Stipdonk, M.J., Chien, W., Anbalagan, V., Bulleigh, K., Hanna, D., Groenewold, G.S.: Gas-phase complexes containing the uranyl ion and acetone. J. Phys. Chem. A. **108**, 10448–10457 (2004)
30. Tatosian, I.J., Iacovino, A.C., Van Stipdonk, M.J.: CID of $[UO_2ClO_4]^+$ revisited: production of $[UO_2Cl]^+$ and subsequent hydrolysis to create $[UO_2OH]^+$. Rapid Commun. Mass Spectrom. **32**, 1085–1091 (2018)
31. Van Stipdonk, M.J., Iacovino, A., Tatosian, I.: Influence of background $H_2O$ on the collision-induced dissociation products generated from $[UO_2NO_3]^+$. J. Amer. Soc. Mass Spectrom. **29**, 1416–1424 (2018)
32. Becke, A.: D. Density-functional thermochemistry. III. The role of exact exchange. J. Chem. Phys. **98**, 5648–5652 (1993)
33. Lee, C., Yang, W., Parr, R.G.: Development of the Colle-Salvetti correlation-energy formula into a functional of the electron density. Phys. Rev. B. **37**, 785–789 (1988)
34. Stephens, P.J., Devlin, F.J., Chabalowski, C.F., Frisch, M.J.: Ab initio calculation of vibrational absorption and circular dichroism spectra using density functional force fields. J. Phys. Chem. **98**, 11623–11627 (1994)
35. Perdew, J.P., Ernzerhof, M., Burke, K.: Rationale for mixing exact exchange with density functional approximations. J. Chem. Phys. **105**, 9982–9985 (1996)
36. Adamo, C., Barone, V.: Toward reliable density functional methods without adjustable parameters: the PBE0 model. J. Chem. Phys. **110**, 6158–6170 (1999)
37. Zhao, Y., Truhlar, D.G.: The M06 suite of density functionals for main group thermochemistry, thermochemical kinetics, noncovalent interactions, excited states, and transition elements: two new functionals and systematic testing of four M06-class functionals and 12 other functionals. Theor. Chem. Accounts. **120**, 215–241 (2008)
38. Frisch, M.J., Trucks, G.W., Schlegel, H.B., Scuseria, G.E., Robb, M.A., Cheeseman, J.R., Scalmani, G., Barone, V., Petersson, G.A., Nakatsuji, H., Li, X., Caricato, M., Marenich, A., Bloino, J., Janesko, B.G., Gomperts, R., Mennucci, B., Hratchian, H.P., Ortiz, J.V., Izmaylov, A.F., Sonnenberg, J.L., Williams-Young, D., Ding, F., Lipparini, F., Egidi, F., Goings, J., Peng, B., Petrone, A., Henderson, T., Ranasinghe, D., Zakrzewski, V.G., Gao, J., Rega, N., Zheng, G., Liang, W., Hada, M., Ehara, M., Toyota, K., Fukuda, R., Hasegawa, J., Ishida, M., Nakajima, T., Honda, Y., Kitao, O., Nakai, H., Vreven, T., Throssell, K., Montgomery Jr., J.A., Peralta, J.E., Ogliaro, F., Bearpark, M., Heyd, J.J., Brothers, E., Kudin, K.N., Staroverov, V.N., Keith, T., Kobayashi, R., Normand, J., Raghavachari, K., Rendell, A., Burant, J.C., Iyengar, S.S., Tomasi, J., Cossi, M., Millam, J.M., Klene, M., Adamo, C., Cammi, R., Ochterski, J.W., Martin, R.L., Morokuma, K., Farkas, O., Foresman, J.B., Fox, D.J.: Gaussian 09, Revision A.02. Gaussian, Inc., Wallingford CT (2016)
39. Glendening, E., Badenhoop, J., Reed, A., Carpenter, J., Bohmann, J., Morales, C., Weinhold, F.: NBO 5.9 G Theoretical Chemistry Institute. University of Wisconsin, Madison (2010)
40. Tian, Z., Kass, S.R.: Carbanions in the gas phase. Chem. Rev. **113**, 6986–7010 (2013)
41. O'Hair, R.A., Rijs, N.J.: Gas phase studies of the Pesci decarboxylation reaction: synthesis, structure, and unimolecular and bimolecular reactivity of organometallic ions. Acc. Chem. Res. **48**, 329–340 (2015)
42. Khairallah, G., da Silva, G., O'Hair, R.A.J.: Molecular salt effects in the gas-phase: tuning the kinetic basicity of $[HCCLiCl]^-$ and $[HCCMgCl_2]^-$ by LiCl and $MgCl_2$. Agnew. Chem. Int. Ed. **53**, 10979–10983 (2014)
43. Woodley, M.J., Khairallah, G.N., da Silva, G., Donnelly, P.S., Yates, B.F., O'Hair, R.A.J.: Role of the metal, ligand, and alkyl/aryl group in the hydrolysis reactions of group 10 organometallic cations $[(L)M(R)]^+$. Organometallics. **32**, 6931–6944 (2013)
44. Błaziak, K., Miller, G.B.S., Ryding, M.J., Uggerud, E.: Reaction model for the formation of benzene from benzoates and Grignard reagents. Eur. J. Org. Chem. 4272–4276 (2017)
45. Van Stipdonk, M., Gresham, G., Groenewold, G., Anbalagan, V., Hanna, D., Chien, W.: Elucidation of the collision-induced dissociation pathways of water and alcohol coordinated complexes containing the uranyl cation. J. Am. Soc. Mass Spectrom. **14**, 1205–1214 (2003)
46. Bartmess, J.E., Scott, J.A., McIver Jr., R.T.: Scale of acidities in the gas phase from methanol to phenol. J. Am. Chem. Soc. **101**, 6046–6056 (1979)
47. Hunter, E.P.L., Lias, S.G.: Evaluated gas phase basicities and proton affinities of molecules: an update. J. Phys. Chem. Ref. Data. **27**, 413–656 (1998)
48. Lyon, J.T., Hu, H.-S., Andrews, L., Li, J.: Formation of unprecedented actinide≡carbon triple bonds in uranium methylidine molecules. Proc. Nat. Acad. Sci. **104**, 18919–18924 (2007)
49. Groenewold, G.S., Cossel, K.C., Gresham, G.L., Gianotto, A.K., Appelhans, A.D., Olson, J.E., Van Stipdonk, M.J., Chien, W.: Binding of molecular $O_2$ to di- and tri-ligated $[UO_2]^+$. J. Am. Chem. Soc. **128**, 3075–3084 (2006)
50. Bryantsev, V.S., Cossel, K.C., Diallo, M.S., Goddard III, W.A., de Jong, W.A., Groenewold, G.S., Chien, W., Van Stipdonk, M.J.: 2-Electron 3-atom bond in side-on ($\eta^2$) superoxo complexes: U(IV) and U(V) dioxo monocations. J. Phys. Chem. A. **112**, 5777–5780 (2008)
51. Lucena, A.F., Carretas, J.M., Marçalo, J., Michelini, M.C., Gong, Y., Gibson, J.K.: Gas-phase reactions of molecular oxygen with uranyl(V) anionic complexes—synthesis and characterization of new superoxides of uranyl(VI). J. Phys. Chem. A. **119**, 3628–3635 (2015)